Shapes, Rotations, Photometric and Internal Properties of Jupiter Trojans

Stefano Mottola[1] · Daniel T. Britt[2] · Michael E. Brown[3] · Marc W. Buie[4] · Keith S. Noll[5] · Martin Pätzold[6]

Abstract

The Jupiter Trojans, being trapped around the stable L4 and L5 Jupiter Lagrangian points, are thought to be more primitive than the Main Belt asteroids. They are believed to have originated from a range of heliocentric distances in the trans-Neptunian region, to have subsequently been scattered inwards, and finally captured in their current location during the phase of Giant Planet migration. As a consequence, their bulk composition is expected to reflect that of the protoplanetary disk at the time and location of their formation. The photometric properties of Trojans appear to have a bi-modal distribution. A few Trojans have been discovered to be binary systems, suspected contact binaries, or to possess moonlets, which has revealed consistently low bulk densities (around 1×10^3 kg m^{-3}) for those systems. Those estimates, together with the presence of a spin barrier between 4 and 4.8 h rotation period, suggest that low densities are a general property of the population, similar to that of cometary nuclei.

Current Trojan physical properties provide clues that relate to their formation that can, in turn, be traced back to the origin of the solar system. We review here our current knowledge on the physical properties of Trojans and the methods used for their determinations. Most of these methods are based on Earth-bound observations, and are limited by the large distance to these objects. The next breakthrough will be made possible by the Lucy mission, which, by visiting several Trojans during a tour through both clouds, will address many open questions and probably raise new ones. The combination of the ground truth for select objects provided by Lucy with the context view given by the Earth-bound observations will result in powerful synergy.

✉ S. Mottola
stefano.mottola@dlr.de

[1] Institute of Planetary Research, DLR, Rutherfordstr. 2, 12489, Berlin, Germany

[2] University of Central Florida, 12354 Research Parkway, Orlando, FL, 32826, USA

[3] Division of Geological and Planetary Sciences California Institute of Technology, Pasadena, CA, 91125, USA

[4] Southwest Research Institute, 1050 Walnut St., Boulder, CO, 80302, USA

[5] NASA Goddard Space Flight Center, 8800 Greenbelt Rd., Greenbelt, MD, 20771, USA

[6] Abteilung Planetenforschung, Rheinisches Institut für Umweltforschung an der Universität zu Köln, Aachenerstrasse 209, 50931 Cologne, Germany

1 Introduction

Jupiter Trojans are a population of bodies trapped at the L4 and L5 Jovian Lagrangian points. The 1:1 mean-motion resonance with Jupiter makes their current orbits stable over the life-time of the Solar System (Emery et al. 2015). The most likely formation scenario of the Trojan clouds involves inward scattering of planetesimals from different zones of the trans-Neptunian region and subsequent capture in the 1:1 resonance with Jupiter. This capture has probably taken place during the migration phase of the Giant Planets during which Jupiter has abruptly changed its semimajor axis due to one or multiple encounters with an ice giant (Morbidelli et al. 2009; Nesvorný et al. 2013; Bottke et al. 2023). This "jumping Jupiter" scenario can potentially explain the current eccentricities of Jupiter and Saturn, and account for the observed number asymmetries that characterize the L4 and L5 Trojan clouds. Due to their dynamical isolation, Jupiter Trojans represent relatively unprocessed samples from the respective formation regions, and their study can help constrain current models about the origin and evolution of the Solar System. The NASA Lucy mission, by visiting several targets in both Trojan clouds, will explore their diversity in terms of composition and physical properties (Levison et al. 2021, 2024).

Due to their distance from Earth, current knowledge about the physical properties of Trojans is still sparse, but has been rapidly progressing in the past decade, mainly due to advances in observational techniques and equipment. In this chapter we review the state of the current knowledge about Jupiter Trojans in terms of their rotations, shapes, masses and densities.

2 Rotation Properties

As of today, reliable spin rates are known for about 240 Trojans with a level of completeness of about 98% down to a diameter of 50 km (Asteroid Lightcurve Database (LCDB), Warner et al. 2009).

Recently, rotation properties of Trojans have been extracted from data from the K2, TESS and Gaia missions (Szabó et al. 2017; Ryan et al. 2017; Pál et al. 2020; Kalup et al. 2021; Ďurech and Hanuš 2023). These spacecraft data, which benefit from uninterrupted observation opportunities covering several weeks – thereby helping reduce the bias that affects ground-based observations and favors short rotation periods (Marciniak et al. 2018) – have considerably increased the size of the sample and confirmed and extended the earlier results.

Previous works (Mottola et al. 2014; French et al. 2015) have noted, based on data available at that time, that the rotation properties of Trojans are different from those of the Main Belt. It was also realized that the distribution of the rotation frequency of Trojans deviates in a statistically significant way from that of a 3-D Maxwellian distribution – the expected end state for a perfectly relaxed population of interacting bodies with random orientation of their spin axes (Harris and Burns 1979). In particular, Trojans show a substantial excess of slow rotators (see Fig. 1) and appear to lack fast-spinning objects, compared to Main Belt Asteroids (MBAs), Mars Crossers (MCs) and Near Earth Objects (NEOs).

Several mechanisms have been proposed for explaining the excess of slow rotators among Trojans. One of those invokes the YORP effect (Rubincam 2000), which is known to effectively act on Main Belt and Near-Earth asteroids. However, Kalup et al. (2021) estimated

Fig. 1 Distribution of the rotation frequency of Jupiter Trojans and of MBAs, MCs and NEOs in the size range 10 - 200 km. 'Dark' refers to objects belonging to the C, P and D taxonomic groups. The letters mark the location in the histogram of the Lucy Trojan targets (P/M= Patroclus-Menoetius; L=Leucus; O=Orus; P=Polymele; E=Eurybates). Data from LCDB (Warner et al. 2009), updated 2023 April
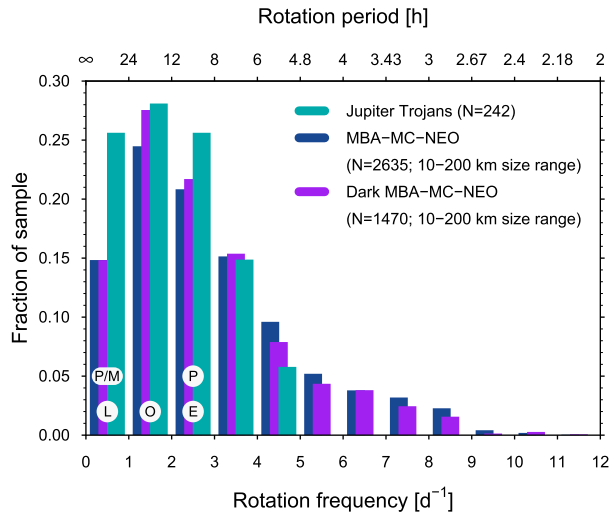
that the typical YORP spin-down time scale for Trojans with a diameter larger than 10 km is ≥ 1 Gyr, which, being much longer than the typical times for spin randomization due to mutual collisions, makes it an unviable mechanism, at least for all but the smallest objects. Another possible explanation is that localized pockets of volatiles in subsurface reservoirs might be sporadically activated, either by minor impacts, or by periodic variations in the heliocentric range, thereby producing a net torque that could spin up or spin down the body (Mottola et al. 2014). A third explanation is that the slow-rotating Trojans were born as similar-size tight binaries – possibly in the transneptunian formation region – and were eventually slowed down due to tidal evolution until they locked in an orbit-synchronous rotation, analogously to the Patroclus-Menoetius system (Nesvorný et al. 2020). Such a system could eventually become either separated, due to impacts or planetary perturbations, or remain intact. In any case, the excess of slow rotators is an interesting feature of the Trojan population that is deserving of additional study. Lucy will contribute to understanding slow rotators by visiting three: the Patroclus-Menoetius synchronous binary system and (11351) Leucus (Mottola et al. 2020), for which no companion has yet been discovered. Also, Lucy will visit the MBA (52246) Donaldjohanson, which will enable a comparison between slow rotators in different environments.

The fastest spin for Trojans for which reliable determinations exist on the LCDB corresponds to a rotation period of about 4.8 h for objects larger than about 10 km (see Fig. 2). Recently, (Chang et al. 2021) conducted a dedicated survey with the Subaru telescope and determined the spin rates of 53 small (2 km $\leq D \leq$ 40 km) Trojans. Three of these objects (with a size between 3.5 and 5 km) appear to spin faster than 4.8 h, with periods ranging from 4.0 h to 4.3 h. These objects, however, were previously unknown and their classification as Trojans is based only on a short-arc determination. It would be therefore desirable to recover those objects and confirm their orbital classification and their rotation periods. Determining the location of the rotational breakup barrier – as in the case of the ~ 2.2 h limit for MBAs, MCs and NEOs – is important because it places a strong constraint on the bulk density of the population, under the assumption that the bodies are cohesionless rubble piles held together by gravity (see Sect. 6). Trojans larger than about 2 km likely belong to this category since they are above the transition zone from "strength-dominated" to "gravity-dominated" bodies, which is thought to occur around a diameter of about 200-400 m (Benz
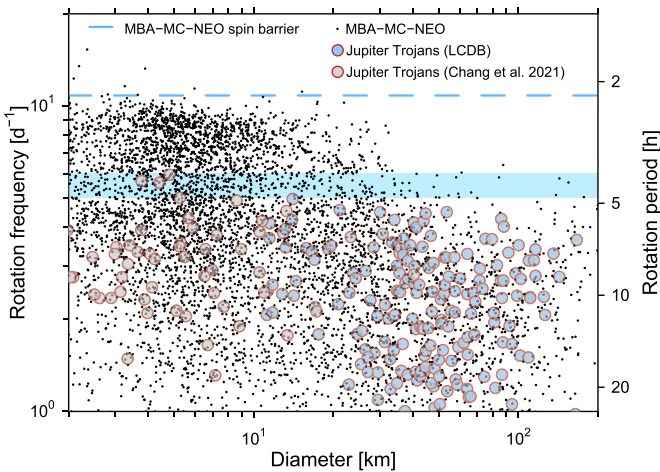
Fig. 2 Scatter plot of the rotation frequency of asteroids vs. their diameter. The horizontal dashed line corresponds to the spin barrier for MBAs, MCs and NEOs at a rotation period of about 2.2 h. Trojan asteroids appear to have a spin barrier between 4 and 4.8 h (shaded area). Data from Chang et al. (2021) and LCDB (Warner et al. 2009), updated 2023 April

and Asphaug 1999). It is to be expected, however, that as soon as the rotations for Trojans in the sub-100-m size range will become measurable, some of those objects, which are likely to be monoliths, will display very short rotation periods.

The distribution of the spin axes of asteroids can provide clues on their formation mechanisms and post-accretion evolution. For example, the tendency for a polarization of the spin axis directions towards the Ecliptic poles has been established for MBAs smaller than 30 km (Hanuš et al. 2016), which has been interpreted as the result of the YORP effect (Rubincam 2000). Also, Cibulková et al. (2016), by determining the spin axis directions of a few thousands of MBAs, have found an asymmetry in the distribution of the Ecliptic longitude of their poles, for which no satisfactory explanation exists to-date.

Until very recently, spin axis orientations for Trojans were only known for about a dozen of objects. As of writing, however, new results based on dense and sparse photometric surveys have been reported in Hanuš et al. (2023). From a sample of 82 objects, the authors find that the distribution of the spin vectors of Trojans in the sky is roughly isotropic. However, the authors also find that the distribution of the orbital obliquity – the angle between the spin vector of an object and its orbital plane – shows an excess of prograde rotators, with a ratio of prograde-to-retrograde of about 1.5. Although there is a 10% probability that the observed asymmetry be due to chance – due to the relatively small size of the sample – their result seems to be compatible with the current understanding of a Trojan formation mechanism driven by streaming instability in a cold trans-Neptunian protoplanetary disk (Youdin and Goodman 2005), which also predicts an excess of primordial prograde rotators. The asymmetry of spins observed for Trojans is smaller than that predicted by numerical simulations of the streaming instability scenario, which is interpreted by Hanuš et al. (2023) as being due to spin randomization during the post-accretion collisional evolution phase.

Fig. 3 The distribution of spectral slopes for 254 Trojan asteroids shows a bi-modal distribution. Modified after Wong et al. (2014)
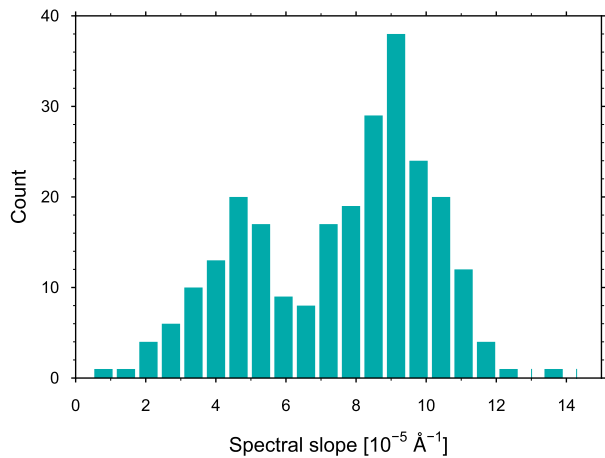
3 Photometric Properties

Studying the photometric properties of planetary surfaces holds the potential of understanding physical properties of their regolith, such as surface porosity, roughness, particle albedo and size distribution. Our current understanding of the photometric properties of Trojans, however, is still quite limited. This is due to the low apparent brightness of most of the objects and to the restricted range of illumination geometries from which they can be observed Earth-bound. As a result, we have accurate and well sampled measurements for a few Trojans, and a large number of less accurate, sparse and serendipitous measurements from systematic observation surveys. The techniques used are disk-integrated photometry, mostly in the form of lightcurves and phase curves, spectrophotometry and spectroscopy.

In addition to providing clues about the location and conditions of formation regions, and of the surface evolutionary history, knowledge of the photometric properties enables the computation of quantities as the albedo and phase integral, which are fundamental for, e.g., computing the thermal balance of the bodies. Compared to MBAs, Trojans have a narrow variety of taxonomic types, being mostly limited to the dark P and D types, and some rare C types (Grav et al. 2012). In turn, the P and D types are very rare in the inner Main Belt. The colors of Trojans mostly cluster in two major groups (Wong et al. 2014; Emery et al. 2024): red and less red (see Fig. 3).

A growing body of observations (Shevchenko et al. 2012; Mottola et al. 2020, 2023) shows that their phase curves are characterized by a very small or absent opposition effect - the non-linear brightness surge usually present on atmosphereless bodies at small phase angles. As a consequence, many Trojans have phase curves with a linear trend down to sub-degree phase angles (Slyusarev and Belskaya 2014). The interpretation of this phenomenon is very likely linked to the relative contributions of the two effects causing the opposition effect: shadow hiding and coherent backscatter. The limited data set, however, does not allow firm answers, with different scholars reaching opposite conclusions (Schaefer et al. 2010; Shevchenko et al. 2012). It is also apparent that the HG photometric system (Bowell et al. 1989), formerly adopted by the IAU and now deprecated, fails to describe the shape of the phase curves of Trojans. On the other hand, the more recently IAU-adopted H, G_1, G_2 system (Muinonen et al. 2010) provides a very good match to Trojans, at least in the limited phase angle range spanned by ground-based observations. Studying the photometric properties of the Trojans, and putting them in the context of other Solar System objects such

as transneptunian objects, comets and giant planets irregular satellites, can help resolve the question of their formation region.

Although less accurate for individual objects, studies of a large number of Trojans through the analysis of serendipitous observations by large-scale surveys provide statistically solid results about the ensemble properties of the population. Schemel and Brown (2021) have analyzed data from the Zwicky Transient Facility (ZTF) survey and established a correlation between colors and phase curves. Working in the HG-System, they found that for phase angles smaller than $12°$, redder objects have systematically higher values of G, while the less-red objects have values closer to the canonical $G = 0.15$ value. Schemel and Brown (2021) suggest that the correlation between color and phase parameter is less likely to be linear, but rather a function of two separate average phase parameters for the two separate color classes of Trojans. They find an average phase parameter values of $G = 0.14 \pm 0.05$ for the less-red cluster of Trojans, which generally corresponds to objects classified as P-type, and $G = 0.22 \pm 0.07$ for the red population, which generally corresponds to objects classified as D-type. Objects classified as C-type have colors only slightly bluer than the less-red population and do not appear to be a clearly distinguishable sub-group, but based on the color correlation they would have phase parameters slightly smaller than those of the less-red population.

4 Shapes

The shapes of asteroids can provide information about the formation mechanisms of these bodies, about the processes that controlled their evolution, and about their physical characteristics. Due to their large geocentric distance, however, even the largest Trojans are beyond, or at the limit of the resolution of current ground-based and Earth co-orbital direct-imaging instruments. A telltale case is (624) Hektor – the largest Trojan – for which, already in the late seventies, Hartmann and Cruikshank (1978) predicted, based on its exceptional maximum lightcurve amplitude of 1.23 mag, a dumbbell shape. Further hypotheses included a close or contact binary. To date, however, a solid description of Hektor's shape is still elusive. Attempts to detect the bilobed nature of Hektor were made by Storrs et al. (1999) with the Hubble Space Telescope (HST) in direct imaging, and by Tanga et al. (2003) with the HST Fine Guidance Sensors in interferometry mode. Neither study, however, could distinguish between the different hypotheses for the shape. Adaptive Optics (AO) observations of Hektor were performed in the near IR by Marchis et al. (2014) between 2006 and 2011 with the 10 m Keck telescope. Those observations seem to show a bilobed shape in some frames, but do not allow distinguishing between a contact or a close binary.

For essentially all Trojans, the most readily available source of information about their shape is given today by photometric lightcurves. The maximum observed amplitude is a first indication about the elongation of the body. Early studies of a limited sample of the largest Trojans (Hartmann et al. 1988) seemed to suggest that Trojans show in average larger lightcurve amplitudes than a sample of similarly sized MBAs. Further data and a bias analysis (Binzel and Sauter 1992) seemed to confirm significantly larger amplitudes only for Trojans larger than 90 km. Later studies, however, based on a much larger sample of Trojans (Mottola et al. 2011), showed no anomalously high amplitudes, suggesting no major differences in the elongation of the MBAs and in the Trojans in the size range 50 - 150 km. More recently, (Schemel and Brown 2021) have compared the amplitudes of Trojans and MBAs in the size range 20 km to 100 km and also found no statistically significant

differences, though the large uncertainties could hide important distinctions between these populations which have yet to be observed.

Close and contact binaries, discussed in more detail by Noll et al. (2023) in this collection, are likely to display above-average amplitudes. For this reason, several studies have searched for binary candidates by identifying objects with large amplitudes in lightcurve surveys (Mann et al. 2007; Sonnett et al. 2015; Ryan et al. 2017). Two large-amplitude Trojans have been identified as likely close or contact binaries based on the incompatibility of their slow-rotation with a dynamically-controlled shape for a fluid-like or rubble-pile object (Mann et al. 2007). Of the survey objects with more sparsely sampled lightcurves, some tens of percent also display high amplitudes and slow rotations, thereby constituting similar contact-binary candidate systems (Sonnett et al. 2015; Ryan et al. 2017). The question remains, however, as to how many of these candidates are really contact binaries, since a large amplitude is not a sufficient condition for binarity (see e.g. Harris and Warner 2020).

A more certain proof for the presence of a binary system and a means for determining its geometry is the detection in the lightcurves of mutual events between well-separated eclipsing companions. The Patroclus-Menoetius system is such a configuration where the two components are orbit-synchronous and undergo periodic mutual event seasons (Buie et al. 2015; Grundy et al. 2018; Wong and Brown 2019; Berthier et al. 2020). Pinilla-Alonso et al. (2022) used observations of seven multiple mutual events occurred in 2017-2018 to identify evidence for a large deviation from a spheroidal shape. Combining these results with those by Buie et al. (2015), suggests that the feature, possibly a large impact basin, must be near the south pole of Menoetius.

Whenever photometric observations are available over a wide range of viewing and illumination geometries, it is possible to reconstruct a 3D convex approximation of the body (Kaasalainen et al. 2001, 2002). This is a robust and established technique that enables the simultaneous determination of the orientation of the body and its "convex hull" shape. Although solutions allowing nonconvexities are also possible, those are in general non-unique if based on lightcurve data alone (Ďurech and Kaasalainen 2003; Viikinkoski et al. 2017). Data fusion with other observational techniques as radar imaging, adaptive optics observations and stellar occultations, however, can help remove the ambiguity in the determination of non-convexities (Viikinkoski et al. 2015). Of those techniques, however, only stellar occultations can be currently successfully applied to Trojans, due to their large geocentric distance.

One of the advantages of the convex inversion technique is that in addition to conventional, densely sampled lightcurve data, it can use also sparse photometric data, as those serendipitously acquired by recent ground- and space-based photometric surveys (Kaasalainen 2004). Although shape and rotation models solely based on sparse data can produce spurious results, the large number of objects for which sparse data are available enables statistical studies to be made and to compare the global properties of different populations. As an example, recent studies have exploited the serendipitous photometric data acquired by the *Gaia* mission (Gaia Collaboration et al. 2018) and the ATLAS photometric survey (Tonry et al. 2018) to derive ellipsoidal or coarse convex shape models of asteroids, among which are also about a dozen of Trojans (Ďurech et al. 2019, 2020). Further results, consisting of convex shape models for additional 71 Trojans have been reported recently (Hanuš et al. 2023; Ďurech and Hanuš 2023).

As mentioned earlier, one complementary technique for the determination of the shape of asteroids that is applicable to the Lucy targets and to Jupiter Trojans in general, is the observation of stellar occultations, which, in recent years, has greatly advanced thanks to the introduction of affordable and high-performance focal plane detectors, the advent of precise

Fig. 4 Shape constraints for Leucus from occultations. The date and subearth longitude is shown for each dataset. All are projected on the plane of the sky at the same scale as observed with no extra geometric corrections. For each event, the formal best-fit ellipse is shown with dotted blue lines. The solid curve that is filled in is a spline curve drawn through the points. The agreement between the ellipse and actual profile is very poor. Occultation data are from Buie et al. (2021)
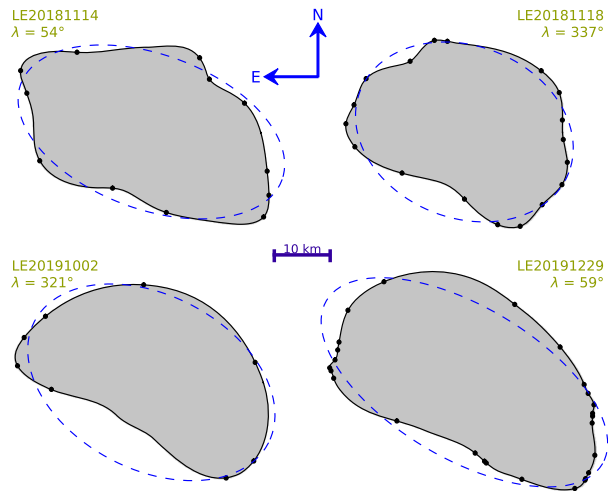
GPS time recording and the availability of accurate all-sky, dense astrometric catalogs. This technique produces a snapshot of the sky projection of the object at the time of the occultation, by sampling its silhouette at discrete positions defined by the chords subtended by the observing stations onto the body. The number of stations on the occultation path defines the density of the silhouette sampling. For this reason, a well sampled object profile calls for the coordinated deployment of a large number of mobile observing stations and the computation of accurate shadow-path predictions (Buie et al. 2015, 2021). This is a field that greatly benefits from the amateur-professional connection, as demonstrated by recent large-scale deployment efforts (Keeney et al. 2022), which, among other things, have resulted in the discovery of a satellite of the Lucy target Polymele.

A common assumption when assessing the shape of a small body from occultation data is to start with the convenience of a tri-axial ellipsoid. The projection of such an ellipsoid is an ellipse and the best-fit ellipse shape is often reported. This ellipse is commonly used both for astrometry derived from the occultation and for a first determination of the geometric albedo. A further approach is to approximate the profile with a continuous function, which can provide a better description of the limb shape, compared to an ellipse. As an example, Fig. 4 shows a collection of profiles for the Lucy target, (11351) Leucus. The data presented in this figure are exactly as reported by Buie et al. (2021). In addition to the fitted ellipses from that work, a spline curve is drawn that satisfies the constraints provided by the occultation data. Although not producing unique profiles, this representation can help identify major features in the body's shape.

Similarly to lightcurve inversion, stellar occultations cannot uniquely resolve concavities on the target, in the sense defined by Viikinkoski et al. (2017). However, if a sufficient number of occultation cross-sections are available, they can describe the shape of those non-convex objects that go under the class of *tangent-covered bodies* or TCBs (Kaasalainen 2011). As an example, these shapes include individually-convex binary systems, dumbbell shapes, banana-shaped objects as (433) Eros or (25143) Itokawa, but not concavities as the large, deep craters on (253) Mathilde.

By obtaining a dense and regular sampling of the limb of a particular target from well-observed occultations at different aspect geometries it is in principle possible to reconstruct the 3D object shape and its spin orientation from occultation data alone. However, it is in general more effective to combine occultation and lightcurve data into one global solution

providing pole direction, shape, absolute size and albedo. Depending on the accuracy and sampling of the data, the shape can be retrieved in its convex (e.g. Ďurech et al. 2011, Mottola et al. 2020, 2023) or nonconvex approximation (Carry et al. 2010; Viikinkoski et al. 2017). Extensive occultation and photometric lightcurve campaigns enabling the application of these methods have been performed and are currently planned for all of the Lucy targets. Lucy, in turn, will return data that will provide an essential set of ground-truth observations from which to further guide our ability to interpret future occultation and photometric data from the rest of the Trojan population.

5 Mass Determination

There are three main methods to determine the mass of a small body in the solar system: 1) by the observation of spacecraft velocity perturbations during a flyby, 2) by observing the gravitational effect on a perturbed asteroid by a planet or a large asteroid, 3) by the astrometric observation of the orbit of a satellite about an asteroid. One fourth possibility is given by the detection of the change of the orbital semi-major axis of an object due to the Yarkovsky nongravitational acceleration (Vokrouhlický et al. 2015) by measuring its astrometric position over many decades. This method has been successfully applied to several NEOs to determine their physical properties, among which their mass. However, since the magnitude of the Yarkovsky drift scales as the Solar irradiation flux and as the inverse of the object's size, its application to Trojan asteroids is currently impractical.

5.1 Spacecraft Flyby

The most precise way to determine masses and, if possible, gravity fields of planetary bodies is the radio tracking of an interplanetary spacecraft flying-by or orbiting the body of interest. The motion of the spacecraft is perturbed by the attracting force of the body acting on the spacecraft, which causes an extra Doppler shift contribution proportional to the projected perturbed velocity vector to be added to the transmitted radio carrier frequency. Essentially, all fundamental information on planetary masses, gravity fields, and internal structure and composition available today was gained by radio tracking experiments.

The very first mass determination of a small body by radio tracking was successfully performed by the NEAR spacecraft for asteroid (253) Mathilde in 1997 (Yeomans et al. 1997) followed by a first determination for NEO (433) Eros during a flyby in 1998 before NEAR eventually entered Eros' orbit in 2000 (Yeomans et al. 1999). Further successful mass determinations of small bodies were conducted by the Japanese orbiter Hayabusa for (25143) Itokawa; by the European comet chaser Rosetta for (21) Lutetia in 2010 (Pätzold et al. 2011); and during the orbital phase around comet 69P/Churyumov-Gerasimenko by Rosetta from 2014 to 2016 (Pätzold et al. 2016, 2019). Those determinations were followed by the gravity investigations by Dawn at Vesta and Ceres (Konopliv et al. 2018) and by OSIRIS-REx at (101955) Bennu – a potentially hazardous asteroid for the Earth (Milani et al. 2009).

The attracting force of a planetary body perturbs the trajectory and velocity of a space-craft flying-by if the body has a sufficiently large mass and the spacecraft is sufficiently close to that body. The radio signal transmitted by the spacecraft will show a total Doppler shift Δf of the radio carrier frequency f_0 proportional to the radial components of the relative spacecraft velocity $v_{s/c,r}$ and the relative perturbed spacecraft velocity $\Delta v_{flyby,r}$ during the

flyby

$$\Delta f = -f_0 \cdot \frac{v_{s/c,r}}{c} - f_0 \cdot \frac{\Delta v_{flyby,r}}{c} \tag{1}$$

$$= -f_0 \cdot \frac{(v_{s/c} + \Delta v_{flyby}) \cdot \cos(\alpha)}{c} \tag{2}$$

where α is the angle between the spacecraft velocity vector $\vec{v_{s/c}}$ and the line-of-sight to Earth, and c is the speed of light. The unperturbed spacecraft velocity $v_{s/c}$ and its Doppler shift can be predicted with high precision for the time of the flyby by the integration of the equation of motion starting with an unperturbed spacecraft state vector many hours before closest approach and considering other non-gravitational forces acting on the spacecraft. The total perturbed spacecraft velocity and Doppler shift Δv_{flyby} and Δf_{flyby}, which are the differences between the pre- and post-encounter values of the respective quantities (measured many hours before and after closest approach), are

$$\Delta v_{flyby} = -2 \cdot \frac{G \cdot M}{v_{s/c} \cdot d} \tag{3}$$

$$\Delta f_{flyby} = -2 \cdot \frac{f_0}{c} \cdot \frac{G \cdot M}{v_{s/c} \cdot d} \cdot \sin(\alpha) \tag{4}$$

where d is the flyby distance. For a two-way radio link, where the uplink signal is transmitted by the ground station, received by the spacecraft and transponded back coherently to the ground station, the two equations above have to be multiplied by a factor of two. The coherent two-way radio link is commonly used in order to take advantage of the superior noise performance of the ground station equipment. The product $G \cdot M$ is derived from the perturbed Doppler shift Δf_{flyby}, which is directly observed, and the known flyby geometry and spacecraft velocity (Pätzold et al. 2001, 2010, 2011, 2014; Andert et al. 2010; Tyler et al. 2008). In the case that the flyby is performed with a binary asteroid or an asteroid with a moon, as Lucy will do for the Trojans Eurybates and its moonlet Queta (Noll et al. 2020) and Polymele and its satellite, provisionally nicknamed Shaun (Buie et al. 2021), both in 2027, and the binary system Patroclus-Menoetius in 2032, the product $G \cdot M$ will represent the total system mass, should it not be possible to track the spacecraft at the time of closest approach.

In order to be able to resolve a sufficiently strong Doppler shift Δf_{flyby} from the background frequency noise, Eq. (4) suggests that the relative flyby velocity $v_{s/c}$ of the spacecraft shall be slow, and that the spacecraft's flyby distance to the target shall be small. The background frequency noise is dominated by the contribution from the propagation of the radio signal though the turbulent solar wind plasma, which induces random phase changes on the radio carrier ("solar plasma noise"). The geometry of the flyby is another important factor for the accuracy of the mass determination: even if $G \cdot M$ is large, the flyby velocity slow and the distance to the object is close, the perturbed velocity vector is still projected into the line-of-sight (LOS) to Earth. If the angle α between the velocity vector of the spacecraft and the LOS is close to the radial direction to Earth, the sine term in Eq. (4) decreases a strong velocity perturbation to a small Doppler shift Δf_{flyby}. The selection of an optimal flyby geometry within the mission constraints makes flyby planning a challenge.

Assuming that the Doppler shift as observed by the ground station could be corrected for other gravitational and non-gravitational forces acting on the spacecraft, Eq. (4) represents

Table 1 Lucy Trojan flyby parameters

Target	r (au)	Δ (au)	Effective diameter (km)	Solar elongation (°)	Fly-by velocity (km s^{-1})	α (°)	Fly-by distance (km)	Doppler shift (MHz)	Nominal GM (10^6 m^3 s^{-2})
Eurybates	5.671	5.623	69	87.5	5.8	108	750 ± 3.0	168 ± 2.2	9.2 ± 1.5%
Polymele	5.688	6.148	21	58.6	6.0	109	434 ± 3.0	13 ± 2.3	0.32 ± 19%
Leucus	5.649	4.891	41	135.2	5.9	69	1000 ± 3.0	21 ± 2.0	2.4 ± 5.2%
Orus	5.342	6.245	61	22.3	7.1	57	1000 ± 3.0	65 ± 2.3	4.9 ± 3.9%
Patroclus/ Menoetius	5.384	5.275	137	90.9	8.1	63	1223 ± 5.0	835 ± 2.1	90 ± 0.5%

r and Δ represent the heliocentric and geocentric distance, respectively. α is the angle between the spacecraft trajectory and the direction to Earth. The nominal GM value is computed for an assumed bulk density of 10^3 kg m^{-3}. The effective diameter is defined as the spherical volume-equivalent diameter. The effective diameter of the Patroclus-Menoetius system corresponds to the sum of the volumes of the two bodies.

the Doppler shift as a response from the attracting force of the asteroid. The following is an estimate of the mass determination accuracy based on Eq. (4)

$$\left(\frac{\sigma_{GM}}{G \cdot M}\right)^2 = \left(\frac{\sigma_{\Delta f_{flyby}}}{\Delta f_{flyby}}\right)^2 + \left(\frac{\sigma_d}{d}\right)^2 + \left(\frac{\sigma_{v_{s/c}}}{v_{s/c}}\right)^2 + (\sigma_\alpha \cdot \tan\alpha)^2 \qquad (5)$$

where $\left(\frac{\sigma_{GM}}{G \cdot M}\right)$ is the fractional accuracy of $G \cdot M$, σ_d is the uncertainty in the flyby distance d, $\sigma_{v_{s/c}}$ is the error in the spacecraft velocity and σ_α is the uncertainty in the geometry angle α. In the case of the Lucy mission, σ_d is estimated by the navigation team as about ±3 km, $\sigma_{v_{s/c}}$ is in the order of ±0.1 mm s^{-1} and σ_α is typically < 0.1°.

Values for Δf, d, $v_{s/c}$ and α for the five Lucy Trojan flybys are listed in Table 1. $\sigma_{\Delta f}$ is the frequency noise as measured in the ground station receiver. It is a combination of the thermal noise of the equipment, the phase noise of the hydrogen maser in the DSN ground station and the plasma noise from the propagation of the radio signal through the turbulent solar wind. The latter dominates the total measured noise $\sigma_{\Delta f}$. The potential solar wind plasma noise was estimated from an analysis of X-band tracking of the Rosetta spacecraft on its way to rendezvous comet 69P/Churyumov-Gerasimenko at 5 au and from the New Horizons spacecraft on its way to Jupiter. A noise range was extrapolated as a function of geocentric distance out to 6 au and as a function of the Sun-Earth-Probe (SEP) angle to the solar disk (Table 1) for each flyby. It is evident that the fractional uncertainty of $G \cdot M$ is dominated by the first two terms in Eq. (5) and amounts to the values in the last column of Table 1. The Lucy project has put a requirement on the Trojan mass determination to be better than 25% (Levison et al. 2021), based on the assumed effective diameters listed in Table 1. Deviations from these assumptions will affect the actual mass accuracy.

5.2 Astrometric Mass Determinations

A further method for estimating the mass of an asteroid is the determination of its gravitational influence on another asteroid or even a planet. As Standish (2000) emphasized, precise mass estimates of the largest asteroids are of fundamental importance, as they currently represent the limiting factor for the accuracy of planetary ephemerides. Baer et al. (2011) presented a list of 60 asteroids with masses estimated from asteroid-asteroid perturbations, from asteroids with moons or binaries and from spacecraft radio tracking during flybys. A

direct comparison of the mass of (21) Lutetia from asteroid-asteroid perturbations (Baer and Chesley 2008; Baer et al. 2011) and the Rosetta flyby in 2010 (Pätzold et al. 2011), however, showed that Lutetia's astrometric mass was overestimated by 50% (against a quoted error of 30%) compared to the highly precise Rosetta flyby mass (with a quoted error of 1%). This inconsistency shows that the method was subjected to a considerable bias. A more recent study by Fienga et al. (2020) attempts to improve the accuracy of perturbation-based mass determinations of asteroids by using prior information about their physical properties and a random Monte Carlo sampling. The comparison of their results with spacecraft-based mass determinations appears promising, with a higher accuracy and smaller systematics than previous methods. A further promising development is anticipated from the Gaia mission, which is expected to improve the orbital accuracy of a large number of asteroids by several orders of magnitude. This improvement, in addition to a corresponding improvement in planetary ephemeris, is expected to result in accurate mass determinations for a few hundreds of asteroids (Mouret et al. 2008).

5.3 Binary Asteroids and Asteroids with a Moon

A direct method for determining the mass of an asteroid is applicable when a satellite or binary companion is identified (Noll et al. 2023). By determining the period T, and semimajor axis a of the satellite, the system mass can be computed using Kepler's third law:

$$M_{sys} = 4\pi^2 a^3 / G T^2$$

Among the Trojans, three systems have had their mass determined in this way. Marchis et al. (2014) determined the mass of (624) Hektor to be $7.9 \pm 1.4 \times 10^{18}$ kg from analysis of the orbit of the small satellite Skamandrios using Keck AO imaging. The mass of the (617) Patroclus-Menoetius binary is well-determined at $M_{sys} = 1.41 \pm 0.03 \times 10^{18}$ kg with the mutual orbit measured with a combination of HST imaging, Keck AO, and astrometry from a stellar occultation (Grundy et al. 2018). Lastly, the mass of (3548) Eurybates and its small satellite, Queta, is now known to be $M_{sys} = 0.151 \pm 0.003 \times 10^{18}$ kg from the satellite's orbit, measured with HST (Brown et al. 2021). The recent discovery by the Lucy Team of a satellite orbiting Polymele (Buie et al. 2022) will probably also result in an accurate mass determination for this system.

High resolution imaging is the most important factor in deriving precise relative astrometry of the primary and satellite needed to determine the orbit. For very small satellites, multiple exposure depths may be required to determine the position of both the primary and secondary. The orbital period may be improved by making repeated observations over longer timescales. Also, by observing the satellite orbit at multiple epochs, the changing geometry of the orbit as viewed from the Earth allows for better constraints of orbital elements other than the period, including the semimajor axis. Over long time scales, non-Keplerian effects may become evident and may be used to obtain the masses of individual objects in a multi-component system (Ragozzine and Brown 2009).

Mass determinations, whether by spacecraft flyby or satellite orbit, inform the determination of density, as discussed in the next section.

6 Densities and Internal Properties

6.1 Current Knowledge About the Density of Trojans from Remote Sensing

Density is a fundamental property of materials that is a function both of composition and structure. For asteroids, bulk density determinations or estimates range from lows of 0.5×10^3 kg m^{-3} and less, about half that of water ice, to as much as 5×10^3 kg m^{-3} or more (Britt et al. 2002; Carry 2012; Scheeres et al. 2015). Among small body populations more similar to Trojans are low-albedo asteroids with satellites in the Outer Main Belt, mostly C-types; these systems have densities of roughly 1.3×10^3 kg m^{-3} (Margot et al. 2015). In the Kuiper Belt, densities skew lower than 1×10^3 kg m^{-3} for binary systems with components smaller than $\sim$500 km in diameter (Grundy et al. 2019). In both of these cases, pore spaces, either macro- or microscopic, must account for a significant fraction of the total volume for the bulk density to be consistent with the density of the compositionally most-likely solids.

There are three Trojan systems for which the mass has been determined, as noted above. The mass uncertainties are $\pm$18% for Hektor and only about $\pm$2% for both Patroclus and Eurybates. The other necessary component for the calculation of the bulk density, the volume, is less well-determined and is usually the limiting factor in density determination (e.g. Carry 2012). The bilobed shape of the primary component in the Hektor system presents a major challenge in determining its volume. Uncertainties in the shape lead to nearly a factor of two difference in density estimates from 1320 ± 530 kg m^{-3} (from Marchis et al. (2014) as corrected by Descamps 2015) to 2430 ± 350 kg m^{-3} (Descamps 2015). For Eurybates, the effective diameter was initially estimated from radiometric observations, and more recently with results from stellar occultations (Keeney et al. 2021). Combined with lightcurve data, a shape model can be used to predict the volume (Mottola et al. 2023). Brown et al. (2021) used a volume of $V = 0.14 \pm 0.04 \times 10^{15}$ m^3 to arrive at a Eurybates bulk density of $\rho = 1100 \pm 300$ kg m^{-3}. For the Patroclus-Menoetius binary Buie et al. (2015) determined the shape of both components from a stellar occultation in 2013 as well as a more recent series of events in 2022 (Keeney et al. 2022) combined with lightcurve data. From the 2013 occultation data and multi-epoch lightcurves, an ellipsoidal shape model with a total volume for both components of $V = 1.36 \times 10^{15}$ m^3 was determined. This volume, combined with the more accurate system mass from Grundy et al. (2018), yields a density of $\rho = 1040$ kg m^{-3}. Unfortunately, Buie et al. (2015) do not cite uncertainties for their shape model, but given the evidence for possible large cratering on Menoetius presented in their work and by Pinilla-Alonso et al. (2022), it is almost certain that the density uncertainty for this system is dominated by the volume uncertainty.

The spin barrier for a population, as shown in Fig. 2, represents the critical rotation rate at which a particle on the equator of the spinning body experiences an apparent centrifugal acceleration that exactly balances the acceleration of gravity (Pravec and Harris 2000). The spin barrier is only meaningful in a statistical sense – if a population that can be assumed to consist of similar objects exhibits a minimum period, it implies that there is a maximum density. In the Main Belt, there is a limit near 2.2 hours which implies a maximum density of 3×10^3 kg m^{-3}. For the Trojans, that limit appears to fall between 4 - 4.8 hours, leading to a maximum density of $\rho_{max} \approx 0.9 \times 10^3$ kg m^{-3} for strengthless rubble-pile Trojans (Ryan et al. 2017; Chang et al. 2021). This limit is marginally consistent with the densities of Patroclus and Eurybates and suggests that the higher density range for Hektor would be not typical for the Trojans as a family.

Overall, low densities would appear to be the norm for Trojans, a result that implies high porosity and also favors ice-rich bulk composition as discussed next. What the Lucy mission

will contribute to the determination of density is the possibility of achieving a more accurate, if not first, system mass and, crucially, a much better volume determination for the Trojans it encounters. If densities can be determined for even a subset of the encountered targets with uncertainties of a few percent, compared to the current tens of percent, it will allow many currently unanswerable questions about composition and structure to be addressed.

6.2 Mineralogies of Trojans and Implications for Their Density and Internal Structure

The mineralogy of the Trojan asteroids is something of an enigma. It is dynamically unlikely that we have any samples of Trojans in the meteorite collections (Bottke et al. 2012; Morbidelli et al. 2010). What clues we do have are based on the typical Trojan low albedo, flat or red spectral slope their low bulk density, and their location outside the frost line in the solar system. The timing of accretion from dust into planets was largely driven by the density of available material.

In the inner regions of the solar system where nebular material densities and temperatures were highest, accretion occurred early and was dominated by high temperature minerals such as silicates and metal, while being depleted in volatiles. The heat from the decay of the short-lived radioactive elements turned the early accreting asteroids into melted balls of liquid rock and metal, or somewhat later accreting asteroids into thermally metamorphosed rocks that were also depleted in volatiles (Hutchison 2004).

Further out in the solar system past the "frost line", lower material densities meant later accretion and produced bodies with lower amounts of short-lived radioactive elements and larger amounts of water ice and organics – the carbonaceous chondrites. Relatively volatile-depleted carbonaceous chondrites like the CVs and the COs have bulk mineralogies similar to ordinary chondrites, but also accreted some volatiles and carbonaceous organics along with enough radioactive elements to produce modest thermal metamorphism.

Accreting later and probably farther out in the solar system are the volatile-rich carbonaceous chondrites, the CM, CR and CI carbonaceous chondrites (Papike 2018). The original mineralogy of these asteroids included silicates such as abundant olivine and pyroxene, along with carbonaceous organics and water ice. They also incorporated modest amounts of radioactive elements, enough to melt accreted ice and drive aqueous metamorphism. The melted ice interacted with the abundant olivine, converting the olivine into the hydrated phyllosilicate serpentine along with a number of other hydrated clay minerals. This had the effect of locking some of the original water into the serpentine crystal structure in the form of hydroxyls. The amount of aqueous alteration, the degree of hydration, the degree of metamorphism, and the local chemical conditions varied hugely in these meteorites and thus the parent bodies (Hutchison 2004; Desch et al. 2018; Hamilton et al. 2019).

Comets probably had a similar accretion history as volatile-rich carbonaceous chondrites in that they accreted a similar mix of high-temperature silicates (olivine and pyroxene), ices, and carbonaceous organics, but with very low amounts of short-lived radioactive isotopes. As a result, they never underwent significant heating or metamorphism and retained their accretional ices including some proportion of supervolatiles, ices such as CO_2, CO, and CH_4 and low-temperature organics (Sitko et al. 2011; Wooden et al. 2017).

Where did the Trojans fit into this accretionary continuum between fully differentiated bodies and almost unprocessed objects like comets? Based on the spectra and physical properties of Trojans there are two possibilities. First, and most likely, the Trojans may be very analogous to comets. They would essentially represent unprocessed outer nebular material and would be under-dense, volatile-rich, and organic rich. The dusty portions of Trojans

would be composed of mixtures of crystalline and amorphous silicates, primarily olivine and pyroxene, along with metal sulfides, carbonates, and perhaps a few clays. The actual proportions of volatiles and dusty components will likely be highly variable since comets can vary in this fraction by a factor of five.

The other alternative is that Trojans accreted with some non-negligible portion of radioactive elements and were altered like CI and CM carbonaceous chondrites. In this scenario the dusty portion to be dominated by the aqueous alteration product serpentine and other hydrated clays. This seems less likely because the process of aqueous alteration would likely compress and consolidate the altered bodies and Trojans exhibit very low-density characteristic of high volatile contents and very little consolidation.

7 Outstanding Questions and Lucy Contributions

With its tour through both Trojan clouds the Lucy mission will help address a number of outstanding questions about the origin and evolution of the Trojans and inform the current Solar System formation models. Through the direct measurement of the volume –via imaging– and of the mass –via the radio science experiment– Lucy will determine the bulk density for all of the Trojan targets, a quantity that bears information about the mineralogy and the structural properties of the bodies. By measuring this quantity for objects of different sizes and belonging to all different taxonomic types present in the Trojan regions, Lucy will look for possible correlations between density, composition and structure. Direct measurements of shape and topography will enable the search for expressions of shape evolution processes as erosion by collision or by sublimation and will enable the application of comparative methods with other bodies previously visited by spacecraft. Accurate measurement of disk-integrated and disk-resolved photometric properties will be possible for observing geometries that are diagnostic and not accessible from Earth. These allow analyses that will complement the geomorphology studies and support the classification of the properties of the surface regolith. Furthermore, they will support the search for regions of possible cometary activity.

Declarations

References

Andert TP, Rosenblatt P, Pätzold M et al (2010) Geophys Res Lett 37:L09202. https://doi.org/10.1029/2009GL041829

Baer J, Chesley SR (2008) Celest Mech Dyn Astron 100:27. https://doi.org/10.1007/s10569-007-9103-8

Baer J, Chesley SR, Matson RD (2011) Astron J 141:143. https://doi.org/10.1088/0004-6256/141/5/143

Benz W, Asphaug E (1999) Icarus 142:5. https://doi.org/10.1006/icar.1999.6204

Berthier J, Descamps P, Vachier F et al (2020) Icarus 352:113990. https://doi.org/10.1016/j.icarus.2020.113990

Binzel RP, Sauter LM (1992) Icarus 95:222. https://doi.org/10.1016/0019-1035(92)90039-A

Bottke WF, Vokrouhlický D, Minton D et al (2012) Nature 485:78. https://doi.org/10.1038/nature10967

Bottke WF, Marschall R, Nesvorný D, Vokrouhlický D (2023). Space Sci Rev 219:83. https://doi.org/10.1007/s11214-023-01031-4

Bowell E, Hapke B, Domingue D et al (1989) In: Binzel RP, Gehrels T, Matthews MS (eds) Asteroids II. University of Arizona Press, Tucson, pp 524–556

Britt DT, Yeomans D, Housen K, Consolmagno G (2002) In: Bottke WF, Cellino A, Paolicchi P, Binzel RP (eds) Asteroids III. University of Arizona Press, Tucson, pp 485–500

Brown ME, Levison HF, Noll KS et al (2021) Planet Sci J 2:170. https://doi.org/10.3847/PSJ/ac07b0

Buie MW, Olkin CB, Merline WJ et al (2015) Astron J 149:113. https://doi.org/10.1088/0004-6256/149/3/113

Buie MW, Keeney BA, Strauss RH et al (2021) Planet Sci J 2:202. https://doi.org/10.3847/PSJ/ac1f9b

Buie MW et al (2022) AAS Division of Planetary Science meeting. Bull Am Astron Soc 54(8):2022n8i512p03

Carry B (2012) Planet Space Sci 73:98. https://doi.org/10.1016/j.pss.2012.03.009

Carry B, Dumas C, Kaasalainen M et al (2010) Icarus 205:460. https://doi.org/10.1016/j.icarus.2009.08.007

Chang C-K, Chen Y-T, Fraser WC et al (2021) Planet Sci J 2:191. https://doi.org/10.3847/psj/ac13a4

Cibulková H, Ďurech J, Vokrouhlický D, Kaasalainen M, Oszkiewicz DA (2016) Astron Astrophys 596:A57. https://doi.org/10.1051/0004-6361/201629192

Descamps P (2015) Icarus 245:64. https://doi.org/10.1016/j.icarus.2014.08.002

Desch SJ, Kalyaan A, Alexander CMO (2018) Astrophys J Suppl Ser 238:11. https://doi.org/10.3847/1538-4365/aad95f

Ďurech J, Hanuš J (2023) Astron Astrophys 675:A24. https://doi.org/10.1051/0004-6361/202345889

Ďurech J, Kaasalainen M (2003) Astron Astrophys 404:709. https://doi.org/10.1051/0004-6361:20030505

Ďurech J, Kaasalainen M, Herald D et al (2011) Icarus 214:652. https://doi.org/10.1016/j.icarus.2011.03.016

Ďurech J, Hanuš J, Vančo R (2019) Astron Astrophys 631:A2. https://doi.org/10.1051/0004-6361/201936341

Ďurech J, Tonry J, Erasmus N et al (2020) Astron Astrophys 643:A59. https://doi.org/10.1051/0004-6361/202037729

Emery JP, Marzari F, Morbidelli A, French LM, Grav T (2015) In: Bottke WF, DeMeo FE, Michel P (eds) Asteroids IV. University of Arizona Press, Tucson, pp 203–220. https://doi.org/10.2458/azu_uapress_9780816532131-ch011

Emery JP, Binzel RP, Britt DT et al (2024). Space Sci Rev 220

Fienga A, Avdellidou C, Hanuš J (2020) Mon Not R Astron Soc 492:589. https://doi.org/10.1093/mnras/stz3407

French LM, Stephens RD, Coley D, Wasserman LH, Sieben J (2015) Icarus 254:1. https://doi.org/10.1016/j.icarus.2015.03.026

Gaia Collaboration, Spoto F, Tanga P et al (2018) Astron Astrophys 616:A13. https://doi.org/10.1051/0004-6361/201832900

Grav T, Mainzer AK, Bauer JM, Masiero JR, Nugent CR (2012) Astrophys J 759:49. https://doi.org/10.1088/0004-637X/759/1/49

Grundy W, Noll K, Buie M, Levison H (2018) Icarus 305:198. https://doi.org/10.1016/j.icarus.2018.01.009

Grundy WM, Noll KS, Buie MW et al (2019) Icarus 334:30. https://doi.org/10.1016/j.icarus.2018.12.037

Hamilton VE, Simon AA, Christensen PR et al (2019) Nat Astron 3:332. https://doi.org/10.1038/s41550-019-0722-2

Hanuš J, Ďurech J, Oszkiewicz DA et al (2016) Astron Astrophys 586:A108. https://doi.org/10.1051/0004-6361/201527441

Hanuš J, Vokrouhlický D, Nesvorný D et al (2023) Astron Astrophys 679:A56. https://doi.org/10.1051/0004-6361/202346022

Harris AW, Burns JA (1979) Icarus 40:115. https://doi.org/10.1016/0019-1035(79)90058-7

Harris A, Warner BD (2020) Icarus 339:113602. https://doi.org/10.1016/j.icarus.2019.113602

Hartmann WK, Cruikshank DP (1978) Icarus 36:353. https://doi.org/10.1016/0019-1035(78)90114-8

Hartmann WK, Binzel RP, Tholen DJ, Cruikshank DP, Goguen J (1988) Icarus 73:487. https://doi.org/10.1016/0019-1035(88)90058-9

Hutchison R (2004) Meteorites. Cambridge University Press, Cambridge

Kaasalainen M (2004) Astron Astrophys 422:L39. https://doi.org/10.1051/0004-6361:20048003

Kaasalainen M (2011) Inverse Probl Imaging 5:37. https://doi.org/10.3934/ipi.2011.5.37

Kaasalainen M, Torppa J, Muinonen K (2001) Icarus 153:37. https://doi.org/10.1006/icar.2001.6674

Kaasalainen M, Mottola S, Fulchignoni M (2002) In: Bottke WF, Cellino A, Paolicchi P, Binzel RP (eds) Asteroids III. University of Arizona Press, Tucson, pp 139–150

Kalup CE, Molnár L, Kiss C et al (2021) Astrophys J Suppl Ser 254:7. https://doi.org/10.3847/1538-4365/abe76a

Keeney B, Buie M, Kaire M et al (2021) In: AGU fall meeting abstracts, vol 2021, pp P32B–03

Keeney B, Buie M, Levison H (Lucy Occultations Team) (2022) In: AAS/Division for planetary sciences meeting abstracts, Vol. 54, 512.04

Konopliv AS, Park RS, Vaughan AT et al (2018) Icarus 299:411. https://doi.org/10.1016/j.icarus.2017.08.005

Levison HF, Olkin CB, Noll KS et al (2021) Planet Sci J 2:171. https://doi.org/10.3847/PSJ/abf840

Levison HF, Marchi S, Noll KS, Olkin CB, Statler TS (2024). Space Sci Rev 220

Mann RK, Jewitt D, Lacerda P (2007) Astron J 134:1133. https://doi.org/10.1086/520328

Marchis F, Ďurech J, Castillo-Rogez J et al (2014) Astrophys J 783:L37. https://doi.org/10.1088/2041-8205/783/2/l37

Marciniak A, Bartczak P, Müller T et al (2018) Astron Astrophys 610:A7. https://doi.org/10.1051/0004-6361/201731479

Margot JL, Pravec P, Taylor P, Carry B, Jacobson S (2015) In: Bottke WF, DeMeo FE, Michel P (eds) Asteroids IV. University of Arizona Press, Tucson, pp 355–374. https://doi.org/10.2458/azu_uapress_9780816532131-ch019

Milani A, Chesley SR, Sansaturio ME et al (2009) Icarus 203:460. https://doi.org/10.1016/j.icarus.2009.05.029

Morbidelli A, Brasser R, Tsiganis K, Gomes R, Levison HF (2009) Astron Astrophys 507:1041. https://doi.org/10.1051/0004-6361/200912876

Morbidelli A, Brasser R, Gomes R, Levison HF, Tsiganis K (2010) Astron J 140:1391. https://doi.org/10.1088/0004-6256/140/5/1391

Mottola S, Di Martino M, Erikson A et al (2011) Astron J 141:170. https://doi.org/10.1088/0004-6256/141/5/170

Mottola S, Di Martino M, Carbognani A (2014) Mem Soc Astron Ital Suppl 26:47

Mottola S, Hellmich S, Buie MW et al (2020) Planet Sci J 1:73. https://doi.org/10.3847/PSJ/abb942

Mottola S, Hellmich S, Buie MW et al (2023) Planet Sci J 4:18. https://doi.org/10.3847/PSJ/acaf79

Mouret S, Hestroffer D, Mignard F (2008) Planet Space Sci 56:1819. https://doi.org/10.1016/j.pss.2008.02.026

Muinonen K, Belskaya IN, Cellino A et al (2010) Icarus 209:542. https://doi.org/10.1016/j.icarus.2010.04.003

Nesvorný D, Vokrouhlický D, Morbidelli A (2013) Astrophys J 768:45. https://doi.org/10.1088/0004-637X/768/1/45

Nesvorný D, Vokrouhlický D, Bottke WF, Levison HF, Grundy WM (2020) Astrophys J 893:L16. https://doi.org/10.3847/2041-8213/ab8311

Noll KS, Brown ME, Weaver HA et al (2020) Planet Sci J 1:44. https://doi.org/10.3847/PSJ/abac54

Noll KS, Brown ME, Grundy WH (2023). Space Sci Rev 219:59. https://doi.org/10.1007/s11214-023-01001-w

Pál A, Szakáts R, Kiss C et al (2020) Astrophys J Suppl Ser 247:26. https://doi.org/10.3847/1538-4365/ab64f0

Papike JJ (ed) (2018) Planetary Materials. De Gruyter, Berlin, Boston. https://doi.org/10.1515/9781501508806

Pätzold M, Wennmacher A, Häusler B et al (2001) Astron Astrophys 370:1122. https://doi.org/10.1051/0004-6361:20010244

Pätzold M, Andert TP, Häusler B et al (2010) Astron Astrophys 518:L156. https://doi.org/10.1051/0004-6361/201014325

Pätzold M, Andert TP, Asmar SW et al (2011) Science 334:491. https://doi.org/10.1126/science.1209389

Pätzold M, Andert TP, Tyler GL et al (2014) Icarus 229:92. https://doi.org/10.1016/j.icarus.2013.10.021

Pätzold M, Andert T, Hahn M et al (2016) Nature 530:63. https://doi.org/10.1038/nature16535

Pätzold M, Andert TP, Hahn M et al (2019) Mon Not R Astron Soc 483:2337. https://doi.org/10.1093/mnras/sty3171

Pinilla-Alonso N, Popescu M, Licandro J et al (2022) Planet Sci J 3:267. https://doi.org/10.3847/PSJ/ac9f11

Pravec P, Harris AW (2000) Icarus 148:12. https://doi.org/10.1006/icar.2000.6482

Ragozzine D, Brown ME (2009) Astron J 137:4766. https://doi.org/10.1088/0004-6256/137/6/4766

Rubincam DP (2000) Icarus 148:2. https://doi.org/10.1006/icar.2000.6485

Ryan EL, Sharkey BNL, Woodward CE (2017) Astron J 153:116. https://doi.org/10.3847/1538-3881/153/3/116

Schaefer MW, Schaefer BE, Rabinowitz DL, Tourtellotte SW (2010) Icarus 207:699. https://doi.org/10.1016/j.icarus.2009.11.031

Scheeres DJ, Britt D, Carry B, Holsapple KA (2015) In: Bottke WF, DeMeo FE, Michel P (eds) Asteroids IV. University of Arizona Press, Tucson, pp 745–766. https://doi.org/10.2458/azu_uapress_9780816532131-ch038

Schemel M, Brown ME (2021) Planet Sci J 2:40. https://doi.org/10.3847/psj/abc752

Shevchenko VG, Belskaya IN, Slyusarev IG et al (2012) Icarus 217:202. https://doi.org/10.1016/j.icarus.2011.11.001

Sitko ML, Lisse CM, Kelley MS et al (2011) Astron J 142:80. https://doi.org/10.1088/0004-6256/142/3/80

Slyusarev IG, Belskaya IN (2014) Sol Syst Res 48:139. https://doi.org/10.1134/S0038094614020063

Sonnett S, Mainzer A, Grav T, Masiero J, Bauer J (2015) Astrophys J 799:191. https://doi.org/10.1088/0004-637x/799/2/191

Standish M (2000) In: Johnston KJ, McCarthy DD, Luzum BJ, Kaplan GH (eds) IAU colloq. 180: Towards models and constants for sub-microarcsecond astrometry, p 120

Storrs A, Weiss B, Zellner B et al (1999) Icarus 137:260. https://doi.org/10.1006/icar.1999.6047

Szabó GM, Pál A, Kiss C et al (2017) Astron Astrophys 599:A44. https://doi.org/10.1051/0004-6361/201629401

Tanga P, Hestroffer D, Cellino A et al (2003) Astron Astrophys 401:733. https://doi.org/10.1051/0004-6361:20030032

Tonry JL, Denneau L, Heinze AN et al (2018) Publ Astron Soc Pac 130:064505. https://doi.org/10.1088/1538-3873/aabadf

Tyler GL, Linscott IR, Bird MK et al (2008) Space Sci Rev 140:217. https://doi.org/10.1007/s11214-007-9302-3

Viikinkoski M, Kaasalainen M, Ďurech J (2015) Astron Astrophys 576:A8. https://doi.org/10.1051/0004-6361/201425259

Viikinkoski M, Hanuš J, Kaasalainen M, Marchis F, Ďurech J (2017) Astron Astrophys 607:A117. https://doi.org/10.1051/0004-6361/201731456

Vokrouhlický D, Bottke WF, Chesley SR, Scheeres DJ, Statler TS (2015) In: Bottke WF, DeMeo FE, Michel P (eds) Asteroids IV. University of Arizona Press, Tucson, pp 509–531. https://doi.org/10.2458/azu_uapress_9780816532131-ch027

Warner BD, Harris AW, Pravec P (2009) Icarus 202:134. https://doi.org/10.1016/j.icarus.2009.02.003

Wong I, Brown ME (2019) Astron J 157:203. https://doi.org/10.3847/1538-3881/ab18f4

Wong I, Brown ME, Emery JP (2014) Astron J 148:112. https://doi.org/10.1088/0004-6256/148/6/112

Wooden DH, Ishii HA, Zolensky ME (2017) Philos Trans R Soc Lond Ser A 375:20160260. https://doi.org/10.1098/rsta.2016.0260

Yeomans DK, Barriot JP, Dunham DW et al (1997) Science 278:2106. https://doi.org/10.1126/science.278.5346.2106

Yeomans DK, Antreasian PG, Cheng A et al (1999) Science 285:560. https://doi.org/10.1126/science.285.5427.560

Youdin AN, Goodman J (2005) Astrophys J 620:459. https://doi.org/10.1086/426895